https://doi.org/10.5194/amt-2022-247
Preprint. Discussion started: 8 September 2022
© Author(s) 2022. CC BY 4.0 License.

Atmospheric Measurement Techniques Discussions

Retrieval of Terahertz Ice Cloud Properties from airborne measurements based on the irregularly shaped Voronoi ice scattering models

Ming Li[1,2], Husi Letu[1], Hiroshi Ishimoto[3], Shulei Li[4], Lei Liu[4], Takashi Y. Nakajima[5], Dabin Ji[1], Huazhe Shang[1], Chong Shi[1]

[1]State Key Laboratory of Remote Sensing Science, Aerospace Information Research Institute, Chinese Academy of Sciences, Beijing, 100101, China
[2]University of Chinese Academy of Sciences, Beijing, 100049, China
[3]Meteorological Research Institute, Japan Meteorological Agency (JMA), Nagamine 1-1, Tsukuba, 305-0052, Japan
[4]College of Meteorology and Oceanography, National University of Defense Technology, Changsha, 410073, China
[5]Research and Information Center (TRIC), Tokai University, 4-1-1 Kitakaname Hiratsuka, Kanagawa, 259-1292, Japan

Correspondence to: Husi Letu (husiletuw@hotmail.com)

Abstract. Currently, the terahertz remote sensing technology is one of the best ways to detect the microphysical properties of ice clouds. Influenced by the representativeness of the ice crystal scattering (ICS) model, the existing terahertz ice cloud remote sensing inversion algorithms still have significant uncertainties. In this study, we developed a terahertz remote sensing inversion algorithm of the ice water path (IWP) and effective particle radius (R_e) of ice clouds based on the Voronoi ICS model. This study utilized the single-scattering properties (extinction efficiency, single-scattering albedo and asymmetry factor) of the Voronoi and Sphere ICS models in the terahertz region. Combined with 14,408 groups of particle size distributions obtained from aircraft-based measurements, we completed the Voronoi and Sphere ICS schemes based on the Voronoi and Sphere ICS models. The two schemes were applied to the RSTAR radiative transfer model to carry out the sensitivity analysis of the top of cloud (TOC) terahertz brightness temperature differences (BTDs) on the IWP and R_e. The sensitivity results showed that the TOC BTDs between 640 and 874 GHz are functions of the IWP, and the TOC BTDs between 380, 640 and 874 GHz are functions of the R_e. The Voronoi ICS scheme possesses stronger sensitivity to the R_e than the Sphere ICS scheme. Based on the sensitivity results, we built a multi-channel look-up table for BTDs. The IWP and R_e were searched from the look-up table using an optimal estimation algorithm. We used 2000 BTD test data randomly generated by the RSTAR model to assess the algorithm' s accuracy. Test results showed the correlation coefficients of the retrieved IWP and R_e reach 0.99 and 0.98, respectively. As an application, we used the inversion algorithm to retrieve the ice cloud IWP and R_e based on the CoSSIR airborne terahertz radiation measurements. Validation against the retrievals of the Bayesian algorithm reveals that the Voronoi ICS model performs better than the Sphere ICS model, with the enhancement of the Mean absolute error of 5.0% and 12.8% for IWP and R_e, respectively. In summary, the results of this study confirmed the practicality and effectiveness of the Voronoi ICS model in the terahertz remote sensing inversion of ice cloud microphysical properties.

https://doi.org/10.5194/amt-2022-247
Preprint. Discussion started: 8 September 2022
© Author(s) 2022. CC BY 4.0 License.

Atmospheric Measurement Techniques Discussions

1 Introduction

Ice clouds account for about 20-30% of the total global cloud mass (Liou, 1992; Rossow and Schiffer, 1991). They play an essential regulatory role in the global radiation balance and the water cycle (Hong et al., 2016; Stephens et al., 2012). Microphysical properties such as the ice water content, ice particle size and shape are the main influencing factors of the scattering and radiative properties of ice clouds (Li et al., 2022; Yi et al., 2017; Zhao et al., 2018; Chen and Zhang, 2018) and, in turn, affect the radiation budget (Heymsfield et al., 2013, 2017; Rossow, 2014). The latest report of the 6th Intergovernmental Panel on Climate Change (IPCC6) (Forster et al., 2021) identifies cloud radiative properties and their feedback effects as the largest source of uncertainty in the overall climate feedback, with errors in ice clouds being one of the most significant factors (Zhang et al., 2021). Therefore, accurate acquisition of microphysical properties of ice clouds is of great importance for studying global climate change and improving the accuracy of numerical model simulations (Baran, 2009, 2012). Remote sensing techniques are one of the most effective means of obtaining microphysical and radiative properties of ice clouds, mainly including ground-based (Cimini et al., 2006), and aircraft-based (Fox et al., 2017) and satellite-based remote sensing observation technologies (Yang et al., 2015, 2018). Currently, large amounts of passive sensors (visible, infrared and microwave detectors) and related ice cloud retrieval algorithms (Nakajima and King, 1990; Nakajima et al., 1991, 2019; Nakajima and Nakajima, 1995; Platnick et al., 2003, 2017; Fox et al., 2019; Brath et al., 2018) have significantly developed. In practice, the current detectors and approaches are confined to a limited range of ice particle sizes (Cho et al., 2015). For example, visible and infrared sensors are only sensitive to small particles smaller than 50 μm (Evans et al., 2005). Additionally, microwave detectors are only useful for large particles larger than 500 μm (Fox et al., 2019). There is a pressing need to develop an effective frequency region for obtaining comprehensive information about ice particles. To bridge the gap between the technologies of visible/infrared and microwave measurement of ice clouds, the terahertz (THz) waves between the infrared and microwave regions have potential advantages of complementing existing visible/infrared and microwave techniques (Gasiewski, 1992).

The terahertz wave is the submillimeter-wave with frequencies in the range of 0.1~10 THz and corresponding wavelengths of 0.03~3mm, comparable to the size of ice particles in ice clouds. Many theoretical studies (Evans and Stephens, 1995a, 1995b; Evans et al., 1998) have shown that the passive terahertz wave has a higher detection capability and sensitivity to the ice water path (IWP) and particle size of ice clouds (Liu et al., 2020). Although terahertz waves were proposed for ice cloud remote sensing in the 1960s (Gao et al., 2016), the technology of terahertz radiometry of ice clouds lagged behind the theory (Evans et al., 2005). It is only within the last decade that terahertz radiometry has been applied to aircraft-based and satellite-based ice cloud remote sensing. With advances in terahertz detectors, researchers have successively developed aircraft-based terahertz radiometers (Gao et al., 2016), such as the Sub-millimeter Wave Cloud Ice Radiometer (SWCIR) (Evans et al., 2002), the Compact Scanning Sub-millimeter wave Imaging Radiometer (CoSSIR) (Evans et al., 2012) and the International Sub-Millimeter wave Airborne Radiometer (ISMAR) (Fox et al., 2017). Also, research institutions have developed satellite-based terahertz radiometers, including Superconducting subMillImeter-wave Limb Emission Sounder (SMILES) (Inatani et

https://doi.org/10.5194/amt-2022-247
Preprint. Discussion started: 8 September 2022
© Author(s) 2022. CC BY 4.0 License.

Atmospheric Measurement Techniques Discussions

al., 2000), Ice Cloud Imager (ICI) (Eriksson et al., 2020; Kangas et al., 2014) and IceCube (Wu et al.), which were proposed in 2013 and are still under development.

Several methods have been reported to retrieve the ice clouds' IWP and particle size from terahertz brightness temperature. Inversion methods can be simply divided into the physical method and linear regression method (Weng et al., 2019). The linear regression method is efficient and convenient, but it lacks a definite physical mechanism and is heavily dependent on the accuracy of the pre-calculated database. The physical method includes the Bayesian algorithm (Evans et al., 2005; Evans et al., 2002), look-up table (LUT) method (Li et al., 2017; Li et al., 2018; Liu et al., 2021) and neural network algorithm (Jimenez et al., 2003). Evans et al. (2002) developed a Monte Carlo Bayesian Integration (MCBI) algorithm to retrieve ice clouds' IWP and median mass diameter (D_{me}) from simulated SWCIR brightness temperatures. Then, Evans et al. (2005) applied the MCBI method to retrieve IWP and D_{me} from the CoSSIR brightness temperatures (referred to as the CoSSIR-MCBI hereafter). The retrievals are validated by the Cloud Radar System data and showed a good agreement of radar backscattering with errors smaller than 5 dB. The physical method is based on the radiative transfer principle and it relies on the forward physical model simulation and effective ice crystal scattering (ICS) model. Different assumptions of ice cloud microphysical properties (shape, size, and particle size distribution of ice particles) in the forward physical model significantly affect the retrieval of the IWP and particle size of ice clouds. Therefore, a practical and representative ICS model is essential for the ice cloud remote sensing in the terahertz region. Evans et al. (1998) used a database of scattering properties of ice particles based on a combination of randomly oriented flat plates, hexagonal prisms and spherical shapes calculated by the DDA method when building the forward model. Li et al. (2016) investigated the effects of five ICS models, namely aggregates, hollow columns, flat plates, rosettes and spheres, on the transmission characteristics of terahertz radiation. The results showed that the ice particle shape could lead to large BTDs. Especially at high frequencies and large particle sizes, particle shape is one of the dominant factors affecting terahertz radiation. Therefore, a typically representative ICS model is the basis for constructing an exact inversion method for the IWP and particle size of ice clouds in the terahertz region.

Many aircraft observations have demonstrated that ice clouds comprise a complex and diverse range of non-spherical ice particles (Lawson et al., 2006, 2019; Liou, 1992). It is still challenging for one specific light-scattering method to precisely calculate the single-scattering properties for non-spherical particles with different size parameters (SZPs). The SZP is the ratio of the equivalent-volume sphere's circumference dimension (or π times particle maximum diameters) to the incident wavelength (Baran, 2012; Nakajima et al., 2009). So far, the light-scattering methods can be roughly divided into the Approximation Method (AM) and the Numerical simulation Method (NM). The AM method is based on ray-tracing techniques, including the Geometrical Optics Method (GOM) (Macke et al., 1996a; Takano and Liou, 1989), which is suitable for large particles. The NM includes the Finite Difference Time Domain (FDTD) (Yang and Liou, 1996b; Yee, 1966) and the Discrete Dipole Approximation (DDA) (Draine and Flatau, 1994; Yurkin and Hoekstra, 2007) methods, which are appropriate for small particles. Combined with the advantages of the AM and NM methods, several improved GOA methods, including the Geometric Optics Integral Equation (GOIE) method (Yang and Liou, 1996a), have been developed. Based on

https://doi.org/10.5194/amt-2022-247
Preprint. Discussion started: 8 September 2022
© Author(s) 2022. CC BY 4.0 License.

Atmospheric Measurement Techniques Discussions

the above-mentioned light-scattering calculation methods, a series of regular-shaped ICS models have been designed, including hexagonal columns, hexagonal plates, bullet rosettes, droxtals and so on (Yang et al., 2000b, 2013; Fu et al., 1999; Takano and Liou, 1989). Considering that the regular-shaped ICS models are not fully representative of the scattering properties of natural ice particles in nature, researchers have developed complex ICS models. Yang et al. (2013) developed the surface-roughened non-spherical ICS models and applied them to the production of MODIS C6 ice cloud products (Platnick et al., 2017). C.-Labonnote et al. (2000, 2001) and Doutriaux-Boucher et al. (2000) developed an ICS database for the Inhomogeneous Hexagonal Monocrystal (IHM) containing embedded inclusions (air bubbles and aerosols). The IHM database was applied to a parameterization scheme for the ice cloud retrievals from the French satellite Polarization and Directionality of the Earth's Reflectance (POLDER) measurements (Deschamps et al., 1994). Unlike the above-mentioned regular-shaped ICS models, Letu et al. (2012) and Ishimoto et al. (2013) analysed ice particles of different shapes and sizes from many NASA aircraft observations and developed an irregular-shaped complex Voronoi ICS model. The single-scattering property database of the Voronoi ICS model in the visible and infrared regions using a combined FDTD, GOIE and GOM approach. The Voronoi ICS model has been adopted for generating official ice cloud products for the Second Generation gLobal Imager (SGLI)/Global Change Observation Mission-Climate (GCOM-C) (Letu et al., 2012, 2016; Nakajima et al., 2019), AHI/Himawari-8 (Letu et al., 2018) and the Multi-Spectral Imager (MSI)/Earth Cloud Aerosol and Radiation Explorer (EarthCARE) satellite programs (Illingworth et al., 2015), which will be launched in 2023. Furthermore, Li et al. (2022) showed the effectiveness of the Voronoi ICS model in describing ice clouds' global visible and infrared radiative properties in the Community Integrated Earth System Mo.,del (CIESM). As a result, researchers have proven the effectiveness and superiority of the database of the Voronoi ICS model in the visible and infrared region in the ice cloud satellite remote sensing and climate model applications (Letu et al., 2016). Recently, Letu et al. (2012) and Ishimoto et al. (2013) have successfully extended the spectral range of the single-scattering property database of the Voronoi ICS model to the terahertz wave region. The database of the Voronoi ICS model in the terahertz region was adopted by Baran et al. (2018) as standard data for the modelling and evaluation of the ICI submillimeter radiometer, which the European Space Agency (ESA) and Met Office jointly developed (Kangas et al., 2014). The results showed good evaluation performance of the Voronoi ICS model. However, the effectiveness of the Voronoi ICS model in the terahertz region in a practical retrieval of ice cloud microphysical properties from terahertz radiation has yet to be discovered.

Motivated by the abovementioned situations, this study aims to apply the Voronoi ICS model to the ice cloud remote sensing retrieval of IWP and particle size from aircraft-based terahertz radiation measurements. To achieve this goal, we use the Voronoi ICS model to create a parameterization scheme (referred to as the Voronoi ICS scheme hereafter) for the ice cloud scattering property in the terahertz region. The Voronoi ICS scheme is employed in the RSTAR radiative transfer model (Nakajima and Tanaka, 1986, 1988) to build the LUT for upward terahertz BTDs at the top of the ice cloud (TOC) between three centre frequencies. The LUT from the Voronoi ICS scheme is compared with that of the Sphere ICS scheme, which is the parameterization scheme made from the Sphere ICS model. The CoSSIR-MCBI algorithm evaluates the retrieval results from both Voronoi and Sphere LUTs. This paper is organised as follows: in Section 2, we introduce the data and radiative

https://doi.org/10.5194/amt-2022-247
Preprint. Discussion started: 8 September 2022
© Author(s) 2022. CC BY 4.0 License.

Atmospheric Measurement Techniques Discussions

transfer model used in this study. Section 3 describes the ice cloud parameterization scheme, retrieval algorithm and the validation with the CoSSIR-MCBI algorithm in detail. Section 4 presents the results of the retrieved IWP and particle size, a comparison of the Voronoi and Sphere ICS schemes and the validation of the retrieval algorithm. Section 5 presents the conclusions of this study.

2 Data and model

2.1 Single-scattering property database for the Voronoi and Sphere models

In this study, we used the single-scattering property database of the Voronoi and Sphere ICS models in the terahertz radiative transfer forward simulation. The database contains 31 ice particle sizes ranging from 0.25 to 9300 μm and covers 20 terahertz channels with frequencies ranging from 10 to 874 GHz, corresponding to 20 wavelengths from 0.03 to 3cm.

The single-scattering properties, including the extinction efficiency, single-scattering albedo and asymmetry factor of the Voronoi and Sphere ICS models in the terahertz region, are used to calculate the terahertz scattering properties of ice clouds. For the Voronoi ICS model, the single-scattering properties are derived from the single-scattering property database developed by Letu et al. (2012, 2016) and Ishimoto et al. (2012) using a combination of FDTD and DDA methods. The DDA method is used to calculate the single-scattering properties of moderate ice particles (SZP>30). The FDTD method is used for small ice particles (SZP<30). The single-scattering property database of the Sphere ICS model is developed based on the exact solution of the Lorentz-Mie theory (Van De Hulst, 1957). The Sphere ICS database contains the same ice particle sizes and terahertz frequencies as the Voronoi ICS database.

2.2 Airborne measurements and auxiliary data

The measured terahertz brightness temperature from CoSSIR/ER-2 aircraft during the TC4 mission on 17 and 19 July 2007 are utilized in this study (available https://espoarchive.nasa.gov/archive/browse/tc4/ER2). During the TC4 field campaign, the CoSSIR measured brightness temperatures in channels from 183.3 to 873.6 GHz (183.3 ± 1.0, 3.0, 6.6, 220, 380.2 ± 1.8, 3.3, 6.2, 640 V, and 874 GHz), all with matched beamwidths about 4° (Evans et al., 2012).

According to the studies by Li et al. (2016) and Liu et al. (2021), the atmospheric windows are near 640 and 874 GHz, and the atmospheric absorption peaks are near 380 GHz. The leading absorbing gases are water vapour and ozone. In this study, we choose the centre frequencies of 380, 640 and 874 GHz. The total water vapour and ozone column data provided by the ERA5 reanalysis data are used as input data for the radiative transfer model to simulate clear-sky brightness temperature. The ERA5 reanalysis data is the fifth generation reanalysis data product developed by the European Centre for Medium-Range Weather Forecasts (ECMWF) (Hans et al., 2019). The total water vapour and ozone column data used have a horizontal resolution of 0.25° × 0.25° and a temporal resolution of 1 hour. The retrieved results are validated against the IWP and D_{me} (Evans et al., 2005) from the CoSSIR-MCBI algorithm during the same period. The IWP and D_{me} are available at https://espoarchive.nasa.gov/archive/browse/tc4/ER2.

https://doi.org/10.5194/amt-2022-247
Preprint. Discussion started: 8 September 2022
© Author(s) 2022. CC BY 4.0 License.

Atmospheric Measurement Techniques Discussions

2.3 Radiative transfer model

The RSTAR radiative transfer model is a set of numerical radiative transfer models developed by Nakajima and Tanaka (1986, 1988) for the plane-parallel atmosphere. The calculated wavelengths can cover from 0.17 to 1000 μm, and the assumed plane-parallel atmosphere could be divided into 50 layers from sea level to a maximum altitude of 120 km. The RSTAR model contains six atmospheric profiles (tropical, mid-latitude summer, mid-latitude winter, high-latitude summer, high-latitude winter, and U.S. standard atmosphere), including vertical profiles of temperature, pressure, water vapor, and ozone. Calculating gas absorption in RSTAR is based on the K-distribution method developed by Sekiguchi and Nakajima (2008), which considers important atmospheric radiative gases (H2O, CO2, O3, N2O, CO CH4, etc.) and trace gases. The K-distribution method parameters were obtained from the HITRAN-2004 database.

3 Method

Figure 1 shows the general flowchart for the inversion of the IWP and effective particle size (R_e) of ice clouds using the CoSSIR brightness temperature measurements. Firstly, based on the single-scattering property database of the Voronoi and Sphere ICS models, the atmospheric radiative transfer model RSTAR is used to build a multi-channel top of cloud (TOC) BTDs LUT for cloudy-sky conditions. Secondly, the RSTAR is used to construct the same channel TOC BTDs LUT for clear-sky conditions with different ozone and water vapour column inputs. Then, the ERA5 reanalysis data is used to estimate the clear-sky TOC BTDs combined with the clear-sky LUT. The measured TOC BTDs between cloudy and clear-sky conditions are obtained using the measured BTDs from the CoSSIR measurements minus the interpolated clear-sky TOC BTDs. Finally, the IWP and R_e are obtained by using Gaussian Newton non-linear optimization estimation method. The retrieved results are validated against the IWP and D_{me} retrieved from the CoSSIR-Evans algorithm. In this study, the R_e is defined by Eq. (1):

$$R_e = \frac{\int_0^\infty r^3 n(r) dr}{\int_0^\infty r^2 n(r) dr}, \quad (1)$$

where r is the equivalent-volume sphere's particle radius. And the D_{me} is given by Eq. (2):

$$D_{me} = \frac{\int_0^\infty Dm(D) n(D) dD}{\int_0^\infty m(D) n(D) dD}, \quad (2)$$

where D is the maximum particle dimension of ice particles, m is the particle mass. To validate our retrieved R_e using the D_{me} from the CoSSIR-Evans algorithm, the transformation from the R_e to the D_{me} is necessary. A statistical multiple linear regression method was used to build a relationship between the R_e and D_{me} over 14,408 PSDs. The R_e of the Voronoi and Sphere ICS models is unified into D_{me} for comparability.

https://doi.org/10.5194/amt-2022-247
Preprint. Discussion started: 8 September 2022
© Author(s) 2022. CC BY 4.0 License.

Atmospheric Measurement Techniques Discussions

3.1 Parameterization of ice cloud optical properties

To apply the Voronoi and spherical ICS models to the RTSAR radiative transfer model for forwarding simulation, two parameterization schemes (Voronoi and Sphere ICS schemes) for the scattering properties of ice clouds in the terahertz spectrum need to be constructed. The ice cloud optical properties depend on the single-scattering properties of the ICS and the particle size distributions (PSDs). The PSDs describe the relationship between ice particle size and particle number concentration and is essential in the calculation of the average scattering properties of ice clouds. In this study, we select 14,408 groups of PSDs from aircraft observation sampling data (available at http://stc-se.com/data/bbaum/Ice_Models/microphysical_data.html) (Heymsfield et al., 2013), which is based on 11 field flight observation experiments covering ice cloud observations in mid-latitude and tropical regions. For the fitting of PSDs for the Voronoi and Sphere ICS models, we adopted the gamma distribution in the form of Eq. (3):

$$n(L) = N_0 L^{\mu} e^{-\lambda L}, \tag{3}$$

where L is the maximum particle dimension, $n(L)$ is the particle concentration per unit volume (e.g., 1/cm^3), N_0 is the intercept, λ is the slope, and μ is the dispersion. The physical meaning of the PSDs is that $n(L)$ times dL is the number of particles per unit area. The effective ice cloud particle size measures the average ice cloud particle size for a given PSD. Different methods have been used to determine the effective ice cloud size, and according to Baum et al. (2005a, 2005b), the effective particle diameter for a given PSD is determined as Eq. (4):

$$D_e = \frac{3}{2}\frac{\int_{L_{min}}^{L_{max}} V(L)n(L)dL}{\int_{L_{max}}^{L_{max}} A(L)n(L)dL}, \tag{4}$$

where D_e is the effective particle diameter, V and A are the volume and projected area of Voronoi and Sphere models. Then, the spectral ice cloud optical properties (mass-averaged extinction coefficients, single-scattering albedo, asymmetry factor and mass-averaged absorption coefficients) for the Voronoi and Sphere ICS schemes are calculated for all PSDs given by Eq. (5)-(8):

$$K_{ext}(\lambda) = \frac{\int_{L_{min}}^{L_{max}} Q_{ext}(\lambda,L)A(L)n(L)dL}{\rho_{ice}\int_{L_{min}}^{L_{max}} V(L)n(L)dL}, \tag{5}$$

$$\varpi(\lambda) = \frac{\int_{L_{min}}^{L_{max}} Q_{sca}(\lambda,L)A(L)n(L)dL}{\int_{L_{min}}^{L_{max}} Q_{ext}(\lambda,L)A(L)n(L)dL}, \tag{6}$$

$$g(\lambda) = \frac{\int_{L_{min}}^{L_{max}} g(\lambda,L)\sigma_{sca}(\lambda,L)n(L)dL}{\int_{L_{min}}^{L_{max}} \sigma_{sca}(L)n(L)dL}, \tag{7}$$

$$K_{abs}(\lambda) = \frac{\int_{L_{min}}^{L_{max}} Q_{abs}(\lambda,L)A(L)n(L)dL}{\rho_{ice}\int_{L_{min}}^{L_{max}} V(L)n(L)dL}, \tag{8}$$

where $K_{ext}(\lambda)$ are spectral mass-averaged extinction coefficients (m^2/g), $\varpi(\lambda)$ is spectral single-scattering albedo, $g(\lambda)$ is spectral asymmetry factor and $K_{abs}(\lambda)$ are spectral mass-averaged absorption coefficients (m^2/g). Q_{ext}, g, Q_{sca} and Q_{abs} are extinction efficiency, asymmetry factor, scattering efficiency and absorption efficiency for Voronoi and Sphere models.

https://doi.org/10.5194/amt-2022-247
Preprint. Discussion started: 8 September 2022
© Author(s) 2022. CC BY 4.0 License.

Atmospheric Measurement Techniques Discussions

Based on the parameterized scattering properties of ice clouds and the effective particle diameter of ice clouds, we developed a parameterization scheme for the scattering properties of ice clouds by establishing the spectral bulk scattering properties of ice clouds as functions of the effective particle diameter of ice clouds. The least squares method is used to obtain first-order and third-order polynomial fitting equations according to Eq. (9)-(12):

$$K_{ext}(\lambda) = a_0 + a_1/D_e \,, \tag{9}$$

$$\varpi(\lambda) = b_0 + b_1 D_e + b_2 {D_e}^2 + b_3 {D_e}^3 \,, \tag{10}$$

$$g(\lambda) = c_0 + c_1 D_e + c_2 {D_e}^2 + c_3 {D_e}^3 \,, \tag{11}$$

$$K_{abs}(\lambda) = d_0 + d_1 D_e + d_2 {D_e}^2 + d_3 {D_e}^3 \,, \tag{12}$$

where a_i, b_j, c_j and d_j (i=0, 1; j=0, 1, 2, 3) are fitting coefficients and are spectral functions of the terahertz wave.

3.2 Look-up table

Before constructing the LUT, the sensitivity analysis of different terahertz brightness temperatures to the IWP and R_e of ice clouds needs to be analyzed to build a representative and efficient LUT. According to the sensitivity results (see section 4.3), the BTDs between the cloudy and clear-sky conditions at 380, 640 and 874 GHz frequencies are simplified to BTD_1, BTD_2 and BTD_3, respectively. And the differences between the two BTDs are represented by a dash. Based on the Voronoi and Sphere ICS schemes, the RSTAR is used to construct two LUTs (Voronoi and Sphere LUT) of $BTD_{2\text{-}3}$ and $BTD_{1\text{-}2}$ - $BTD_{2\text{-}3}$ for cloudy and clear-sky conditions. For the cloudy-sky LUT, the number of the IWP is set to 12, and the range of values is defined in log10 space from 0 to 3.36 in steps of 0.28. The number of R_e is set to 6, and the range of values is defined in log10 space from 1.6 to 3.1 in steps of 0.25. For the clear-sky LUT, the number of total ozone columns is set to 7, and the range of values is from 200 to 500 in steps of 50. To be consistent with aircraft observations of terahertz brightness temperatures, $BTD_{2\text{-}3}$ and $BTD_{1\text{-}2}$ - $BTD_{2\text{-}3}$ are simulated at the mean altitude (20 km). The U.S. standard atmospheric profile is used in the simulation, and the cloud top temperature is assumed to be the same as the atmospheric temperature at that level. The surface is assumed to be a black body (emissivity equals 1) with a temperature of 288.15 K.

3.3 Optimal estimation inversion method

Based on the terahertz BTDs LUTs for the Voronoi and Sphere ICS schemes established in the previous section, the IWP and R_e are retrieved using an optimization method with Gaussian Newtonian nonlinear iterations. Based on the atmospheric radiative transfer transmission in the terahertz spectrum, if the background field under clear-sky conditions is subtracted from the cloudy-sky condition, the TOC BTDs are only functions of the cloud microphysical property parameters, which are given by Eq. (13)-(14):

$$Y = F(X) \,, \tag{13}$$

$$X = \begin{pmatrix} IWP, \\ re \end{pmatrix}, Y = \begin{pmatrix} BTD_{2-3}, \\ BTD_{1-2} - BTD_{2-3} \end{pmatrix}, \tag{14}$$

https://doi.org/10.5194/amt-2022-247
Preprint. Discussion started: 8 September 2022
© Author(s) 2022. CC BY 4.0 License.

Atmospheric Measurement Techniques Discussions

where X is the vector-matrix composed of the variables of the IWP and R_e to be solved and Y is the vector composed of the two BTDs. Assuming that Y is the value of two BTDs measured by the aircraft, the inverse X is the minimum value for solving Eq. (15):

$$J(X) = min\{\|y - F(X)\| + \gamma\|X - X_a\|\}, \quad (15)$$

where X_a is a vector consisting of the prior estimates of the IWP and R_e, γ is a Lagrangian operator, min denotes the minimal value of solving this function, and the value of X at the minimal value is considered as the retrieved result. For the solution method of the nonlinear problem in the inversion process, the Newton nonlinear iterative method is usually used. It has a faster inversion speed and higher solution accuracy, and its iterative form follows Eq. (16):

$$X_{i+1} = X_i - J''(X_i)^{-1}J'(X_i), \quad (16)$$

where the i represents the number of iterations, and the superscripts denote the first-order and second-order derivations, then the iterations start from the a priori initial estimate until the convergence criterion is satisfied or when the number of iterations satisfies the required number of iterations, then the iteration is stopped, and the solution results are obtained. The final inversion results are validated using the results from the CoSSIR-MCBI algorithm.

4 Results

4.1 Single-scattering property database for the Voronoi and Sphere models

Figure 2 compares the extinction efficiency, single-scattering albedo and asymmetry factor, varying with the SZP for the Voronoi and Sphere models at 325 and 874 GHz. For small ice particles less than 120 μm, the single-scattering properties are small and barely influenced by the shape of ice particles. This is because the single-scattering properties of ice particles are close to Rayleigh scattering when the SZP is small. The single-scattering properties of the Voronoi model vary more smoothly than those of the Sphere model. This reflects that FDTD and DDA methods provide good continuity for the transition between different size parameters of the Voronoi model.

Figure 3 shows the contours of the single-scattering properties for the Voronoi and Sphere models over 20 terahertz wavelengths and 31 particle sizes. The sharp changes in the single-scattering properties for the Voronoi and Sphere models can be seen from small to large ice particles. For the Voronoi and Sphere models, small particles in the low-frequency channels are mainly Rayleigh scattering with significant absorption effects. The absorption energy is proportional to the volume of ice particles and is barely affected by the ice particle shape. In the high-frequency channels, the Mie-scattering plays a leading role, and the scattering function plays a dominant role. Especially for large ice particles, the single-scattering albedo is close to one, and the influence of the ice particle shape becomes obvious. Overall, the extinction efficiency and single-scattering albedo of the Voronoi model are higher than that of the Sphere model in the high-frequency channel for large ice particles. The asymmetry factor of the Voronoi model is higher than that of the Sphere model in the low-frequency channel for large ice particles.

https://doi.org/10.5194/amt-2022-247
Preprint. Discussion started: 8 September 2022
© Author(s) 2022. CC BY 4.0 License.

Atmospheric Measurement Techniques Discussions

Figure 4 displays the scattering phase functions of the Voronoi and Sphere models. The variation of the scattering phase function for the Voronoi model tends to be smooth compared to the Sphere model. The scattering phase function is axisymmetric about the 90° scattering angle for small ice particles, which can be approximated as Rayleigh scattering. For small ice particles, the scattering shows extreme values in the forward (0°) and backward (180°) directions and shows minimal values in both side (90° and 270°) directions. As the size of ice particles increases, the forwarding scattering is significantly larger than the side and backward scattering and gradually tends to be more Mie-scattering. For the Sphere model in the high-frequency channels, the forward scattering increases with the increase in particle size. In the low-frequency channels, the forward scattering remains almost constant with the increase in particle size. Compared to the Sphere model, the Voronoi model shows more significant variations of the phase functions. For the Voronoi model, the low values of the scattering phase function move towards large scattering angles with the increase in particle size.

4.2 Bulk scattering properties of ice clouds in the terahertz region

Based on the single-scattering properties of the Voronoi and Sphere ICS models, the Voronoi and Sphere ICS schemes are developed in the terahertz region with the integration over both PSDs and terahertz frequencies. The calculated bulk scattering properties include the mass extinction coefficients, single-scattering albedo, asymmetry factor and mass absorption coefficients. Figure 5 shows the bulk scattering properties of the Voronoi ICS scheme and their differences between the Voronoi and Sphere ICS schemes over 14,408 PSDs at four terahertz frequencies (325, 448, 664 and 874 GHz). The bulk scattering properties of ice clouds depend on the effective diameter and terahertz frequency. The single-scattering albedo increases linearly with the effective diameter for the Sphere ICS scheme. For the Voronoi ICS scheme, the single-scattering albedo increases for the effective diameter smaller than 100 μm and approaches 0.95 with effective diameters exceeding 100 μm. The mass extinction coefficients obtained from the two schemes show a uniformly positive correlation with the effective diameter and terahertz frequency. The Voronoi ICS scheme has higher mass extinction coefficients than the Sphere ICS scheme for effective diameters less than 50 μm except at 874 GHz. When the effective diameter is larger than 50 μm, the Voronoi ICS scheme has weaker mass extinction coefficients than the Sphere ICS scheme with the increase of the effective diameter at four terahertz frequencies. For effective diameters larger than 80 μm, the asymmetry factor of the Voronoi ICS scheme is larger than that of the Sphere ICS scheme. For effective diameters larger than 50 μm, the mass absorption coefficients of the Sphere ICS scheme are stronger than those of the Voronoi ICS scheme. For both schemes, the bulk scattering properties increase with increasing frequencies.

4.3 Sensitivity results

We discuss the sensitivity of the TOC BTD_2 and $BTD_{2\text{-}3}$ to the IWP and R_e based on the Voronoi and Sphere ICS scheme in the RSTAR model. Figure 6 shows that the BTD_2 and $BTD_{2\text{-}3}$ are positively correlated with the IWP and R_e. The BTD_2 and $BTD_{2\text{-}3}$ shows a monotonically increasing relationship with the IWP. For ice clouds with the IWP smaller than 200 g/m^2, the 50 to 1000 μm particle sizes can lead to 0-10 K BTD_2 and 0-6 K $BTD_{2\text{-}3}$. The BTD_2 and $BTD_{2\text{-}3}$ increases with the increase

https://doi.org/10.5194/amt-2022-247
Preprint. Discussion started: 8 September 2022
© Author(s) 2022. CC BY 4.0 License.

Atmospheric Measurement Techniques Discussions

of the R_e for R_e less than 200 μm and is close to a constant value for R_e larger than 200 μm. Compared to the Sphere ICS scheme, the Voronoi ICS scheme has higher BTD_2 and $BTD_{2\text{-}3}$, and their differences is proportional to the IWP and R_e. In summary, the TOC BTD_2 and $BTD_{2\text{-}3}$ has a strong sensitivity to the IWP and R_e, especially for moderate to large ice particles and large IWPs.

Figure 7 exhibits the variation of the TOC BTDs at different IWPs and R_e for 380, 640 and 874 GHz frequencies based on the RSTAR model. The BTDs of 380, 640 and 874 GHz frequencies have a strong sensitivity to the IWP, and increase with the increase of the IWP, and the slope shows that the increase is pronounced when the IWP is less than 600 g/m^2. The BTDs between 640 and 874 GHz frequencies have a strong sensitivity to the R_e and increase with the increase in the R_e. By comparing the LUTs of the Voronoi and Sphere ICS models, it is found that the IWP of the Sphere LUT is higher than that of the Voronoi LUT for the same BTDs between 640 and 874 GHz frequencies. The R_e of the Sphere LUT is smaller than that of the Voronoi LUT for the same BTDs between 380, 640 and 874 GHz frequencies. This is mainly due to the higher single-scattering albedo and asymmetry factor of the Voronoi ICS model at low frequencies, resulting in stronger forward scattering energy and a smaller BTD than the Sphere ICS model for the same IWP and R_e.

4.4 Inversion results

Figure 8 shows the validation results of the inversion algorithm using 2000 groups of $BTD_{2\text{-}3}$ and $BTD_{1\text{-}2}$-$BTD_{2\text{-}3}$ simulated by RSTAR using 2000 randomly generated IWP and R_e. The results show that most of the validation results of the red density lie on the 1:1 line. The correlation coefficients of the IWP and R_e are 0.94 and 0.99, and the mean absolute errors (MAE) are 35.46 g/m^2 and 8.56 μm, respectively. The high accuracy of the validation results proves the effectiveness and accuracy of the inversion algorithm.

As illustrated in Figure 9, our retrieval results of the IWP and D_{me} match with the CoSSIR-MCBI results on 19 July 2007. The matching rates for the IWP and D_{me} are 80.3% and 83.2%, respectively. Figure 10 shows the inversion results of IWP and R_e based on the optimal estimation algorithm from the CoSSIR aircraft measured brightness temperature. For the Voronoi and Sphere ICS model, the correlation coefficients of the retrieved IWP are 0.87 and 0.67, with MAEs of 22.38 g/m^2 and 23.55 g/m^2 and RMSE of 30.45 g/m^2 and 35.22 g/m^2, respectively. The correlation coefficients of the R_e are 0.83 and 0.64, with MAEs of 18.46 μm and 21.19 μm and RMSE of 24.57 μm and 26.51 μm, respectively. Overall, the accuracy for the IWP and R_e based on the Voronoi ICS model is better than that of the Sphere ICS model compared to the CoSSIR-MCBI algorithm. The Sphere ICS model overestimates IWP and R_e compared with the validation data.

5 Conclusions

In this study, we applied the irregular-shaped Voronoi ice crystal scattering (ICS) model to the ice cloud remote sensing retrieval of the ice water path (IWP) and particle size based on the Compact Scanning Sub-millimeter wave Imaging Radiometer (CoSSIR) terahertz radiation measurements. The bulk scattering property parameterization (Voronoi ICS

https://doi.org/10.5194/amt-2022-247
Preprint. Discussion started: 8 September 2022
© Author(s) 2022. CC BY 4.0 License.

Atmospheric Measurement Techniques Discussions

scheme) in the terahertz region was completed based on the single-scattering properties of the Voronoi ICS database and 14,408 groups of particle size distributions from in-situ observations. The Voronoi ICS scheme was applied to the atmospheric radiative transfer model RSTAR and compared with the Sphere ICS scheme to carry out the sensitivity analysis. We conducted the sensitivity analysis of brightness temperature differences (BTDs) between 380, 640 and 874 GHz to the IWP and particle size. Based on the sensitivity analysis results, we built two terahertz BTD look-up tables (LUT) for both the Voronoi and Sphere ICS schemes using the RSTAR atmospheric radiative transfer model. Based on the two LUTs, we utilized the Gaussian Newton non-linear optimization estimation method to retrieve the IWP and particle size from the CoSSIR terahertz radiation measurements. Finally, the retrieval results were evaluated by the IWP and median mass diameter (D_{me}) retrieved using the CoSSIR-MCBI algorithm. The main conclusions were obtained as follows.

The bulk scattering properties of ice clouds in the terahertz region, including the mass extinction coefficients, single-scattering albedo, asymmetry factor and mass absorption coefficients of the Voronoi ICS scheme, were applied to the RSTAR model and were compared with the Sphere ICS scheme. The results showed that the Voronoi ICS scheme has a distinct feature of lower absorption properties and higher asymmetry factors for larger effective diameters in the terahertz region. This feature could be related to the complex, multifaceted shape of the Voronoi ICS model and suggests that the Voronoi ICS scheme can produce relatively stronger forward scattering and fewer absorption effects compared with the Sphere ICS scheme.

The sensitivity analysis showed that the BTDs between 640 and 874 GHz are sensitive to the IWP variation, and the BTDs between 380, 640 and 874 GHz are sensitive to the particle size. The atmospheric absorption peak near 380 GHz and the atmospheric window near the 640 and 874 GHz can be effectively used for the IWP in the range of 50-200 g/m^2 and particle size of 50-300 μm.

A comparison of the results from the Voronoi and Sphere ICS models shows that the results from the Voronoi ICS model are better than the Sphere ICS model. For the Voronoi ICS model, the mean absolute error (MAE) of the IWP and D_{me} is improved by 5.0% and 12.8%, and RMSE is improved by 13.5% and 7.3%, respectively. The Sphere ICS scheme overestimates the IWP and D_{me} by up to the MAE of 23.55 g/m^2 and 21.19 μm, respectively. This is mainly due to the differences in the absorption efficiency and asymmetry factor in the single-scattering properties of ice particles, which have a significant impact on the description of the scattering and radiative properties of ice clouds in the terahertz region.

In conclusion, the analysis of terahertz BTDs between 380, 640 and 874 GHz exhibits obvious sensitivity to the IWP and particle size of ice clouds, which could complement visible/infrared and microwave spectra. The present work provides the potential utility of inferring the IWP and particle size of ice clouds using BTDs between 380, 640 and 874 GHz. With the LUT for BTDs between 380, 640 and 874 GHz, the retrieval of terahertz ice cloud properties from airborne measurements based on the irregularly-shaped Voronoi ICS models is newly completed. We find that the retrieval results based on the Voronoi ICS scheme present a better agreement with the CoSSIR-MCBI algorithm than the Sphere ICS scheme. This study confirmed that the Voronoi ICS model has ice cloud inversion capabilities in the terahertz region, which may provide a reference for future use in aircraft-based and satellite-based terahertz ice cloud remote sensing applications.

https://doi.org/10.5194/amt-2022-247
Preprint. Discussion started: 8 September 2022
© Author(s) 2022. CC BY 4.0 License.

Atmospheric Measurement Techniques Discussions

Data availability

The CoSSIR/ER-2 aircraft data during the TC4 mission on 17 and 19 July 2007 are available at https://espoarchive.nasa.gov/archive/browse/tc4/ER2. The IWP and D_{me} from the CoSSIR-MCBI algorithm are available at https://espoarchive.nasa.gov/archive/browse/tc4/ER2. The 14,408 groups of PSDs from 11 field flight observation experiments are available at http://stc-se.com/data/bbaum/Ice_Models/microphysical_data.html.

Author contribution

Ming Li developed the terahertz ice cloud remote sensing inversion algorithm for the IWP and particle size of ice clouds and evaluated the retrieval result by validating it against the results from the CoSSIR-MCBI algorithm. Ming Li is also responsible for downloading auxiliary data and writing the initial draft of this manuscript.

Husi Letu provided the single-scattering property database of Voronoi models in the terahertz region and assisted in developing the parameterization of ice cloud scattering properties in the RSTAR model. Husi Letu also designed the aims and structures of this study and guided the writings and revisions of the manuscript.

Hiroshi Ishimoto developed the single-scattering property database of Voronoi models in the terahertz region and helped in the writings and revisions of the manuscript.

Takashi Y. Nakajima provided the atmospheric radiative transfer model RSTAR and is responsible for the optimization of the RSTAR model and assisted in the parameterization of ice cloud scattering properties.

Shulei Li and Lei Liu assisted in developing the ice cloud remote sensing retrieval algorithm of the IWP and particle size of ice clouds and provided the CoSSIR terahertz radiation measurement data, as well as helped with reviewing the manuscript.

Dabin Ji guided the development of the ice cloud remote sensing retrieval algorithm and helped with the review of the manuscript.

Huazhe Shang assisted in analyzing the results and guided the flowchart of the study, as well as reviewed the manuscript.

Chong Shi assisted in designing the structures of this study, guided the writings of the paper and helped review the manuscript.

Competing interests

The authors declare that they have no conflict of interests.

Acknowledgement

This work is supported by the National Natural Science Foundation of China (Grant No. 42025504).

https://doi.org/10.5194/amt-2022-247
Preprint. Discussion started: 8 September 2022
© Author(s) 2022. CC BY 4.0 License.

Atmospheric Measurement Techniques Discussions

References

Baran, A., Ishimoto, H., Sourdeval, O., Hesse, E., and Harlow, C.: The applicability of physical optics in the millimetre and sub-millimetre spectral region. Part II: Application to a three-component model of ice cloud and its evaluation against the bulk single-scattering properties of various other aggregate models, Journal of Quantitative Spectroscopy and Radiative Transfer, 206, doi:10.1016/j.jqsrt.2017.10.027, 2018.

Baran, A. J.: A review of the light scattering properties of cirrus, J Quant Spectrosc Ra, 110, 1239-1260, doi:10.1016/j.jqsrt.2009.02.026, 2009.

Baran, A. J.: From the single-scattering properties of ice crystals to climate prediction: A way forward, Atmos Res, 112, 45-69, doi:10.1016/j.atmosres.2012.04.010, 2012.

Baum, B. A., Heymsfield, A. J., Yang, P., and Bedka, S. T.: Bulk scattering properties for the remote sensing of ice clouds. Part I: Microphysical data and models, J Appl Meteorol, 44, 1885-1895, doi:10.1175/JAM2308.1, 2005a.

Baum, B. A., Yang, P., Heymsfield, A. J., Platnick, S., King, M. D., Hu, Y. X., and Bedka, S. T.: Bulk scattering properties for the remote sensing of ice clouds. Part II: Narrowband models, J Appl Meteorol, 44, 1896-1911, doi:10.1175/JAM2309.1, 2005b.

Brath, M., Fox, S., Eriksson, P., Harlow, C., Burgdorf, M., and Buehler, S.: Retrieval of an ice water path over the ocean from ISMAR and MARSS millimeter and submillimeter brightness temperatures, Atmospheric Measurement Techniques, 11, 611-632, doi:10.5194/amt-11-611-2018, 2018.

C.-Labonnote, L., G., Brogniez, J.-C., Buriez, M., Doutriaux-Boucher, J.-F. Gayet, and A. Macke: Polarized light scattering by inhomogeneous hexagonal monocrystals: Validation with ADEOS-POLDER measurements, J Geophys Res-Atmos, 106, 12139-12153, doi:10.1029/2000JD900642, 2001.

C.-Labonnote, L., Brogniez, G., Doutriaux-Boucher, M., Buriez, J.-C., Gayet, J.-F., and Chepfer, H.: Modeling of light scattering in cirrus clouds with inhomogeneous hexagonal monocrystals. Comparison with in-situ and ADEOS-POLDER measurements, Geophysical Research Letters - GEOPHYS RES LETT, 27, 113-116, doi:10.1029/1999GL010839, 2000.

Chen, Q. and Zhang, H.: Effects of ice crystal habit weight on ice cloud optical properties and radiation, Acta Meteorologica Sinica, 76, 279-288, doi:10.11676/qxxb2017.088, 2018.

Cho, H.-M., Zhang, Z., Meyer, K., Lebsock, M., Platnick, S., Ackerman, A. S., Di Girolamo, L., C.-Labonnote, L., Cornet, C., Riedi, J., and Holz, R. E.: Frequency and causes of failed MODIS cloud property retrievals for liquid phase clouds over global oceans, Journal of Geophysical Research: Atmospheres, 120, 4132-4154, doi:10.1002/2015JD023161, 2015.

Cimini, D., Westwater, E., Gasiewski, A., Klein, M., Leuski, V., Mattioli, V., Dowlatshahi, S., and Liljegren, J.: Ground-Based Millimeter- and Submillimiter Wave Observations of the Arctic Atmosphere, 247-251 pp., doi:10.1109/MICRAD.2006.1677097, 2006.

Deschamps, P. Y., Breon, F. M., Leroy, M., Podaire, A., Bricaud, A., Buriez, J. C., and Seze, G.: The POLDER Mission: Instrument Characteristics and Scientific Objectives, Ieee T Geosci Remote, 32, 598-615, doi:10.1109/36.297978, 1994.

© Author(s) 2022. CC BY 4.0 License.


Doutriaux-Boucher, M., Buriez, J.-C., Brogniez, G., C.-Labonnote, L., and Baran, A.: Sensitivity of retrieved POLDER directional cloud optical thickness to various ice particle models, Geophysical Research Letters - GEOPHYS RES LETT, 27, 109-112, doi:10.1029/1999GL010870, 2000.

Draine, B. T. and Flatau, P. J.: Discrete-Dipole Approximation for Scattering Calculations, J Opt Soc Am A, 11, 1491-1499, doi:10.1364/JOSAA.11.001491, 1994.

Eriksson, P., Rydberg, B., Mattioli, V., Thoss, A., Accadia, C., Klein, U., and Buehler, S.: Towards an operational Ice Cloud Imager (ICI) retrieval product, Atmospheric Measurement Techniques, 13, 53-71, doi:10.5194/amt-13-53-2020, 2020.

Evans, K., Wang, J., Racette, P., Heymsfield, G., and Li, L.: Ice Cloud Retrievals and Analysis with the Compact Scanning Submillimeter Imaging Radiometer and the Cloud Radar System during CRYSTAL FACE, Journal of Applied Meteorology - J APPL METEOROL, 44, 839-859, doi:10.1175/JAM2250.1, 2005.

Evans, K., Wang, J., Starr, D., Heymsfield, G., Li, L., Tian, L., Lawson, R., Heymsfield, A., and Bansemer, A.: Ice hydrometeor profile retrieval algorithm for high-frequency microwave radiometers: Application to the CoSSIR instrument during TC4, Atmospheric Measurement Techniques, 5, 2277-2306, doi:10.5194/amt-5-2277-2012, 2012.

Evans, K. F. and Stephens, G. L.: Microwave Radiative Transfer through Clouds Composed of Realistically Shaped Ice Crystals. Part I. Single Scattering Properties, Journal of Atmospheric Sciences, 52, 2041-2057, doi:10.1175/1520-0469(1995)052<2041:MRTTCC>2.0.CO;2, 1995a.

Evans, K. F. and Stephens, G. L.: Microweve Radiative Transfer through Clouds Composed of Realistically Shaped Ice Crystals. Part II. Remote Sensing of Ice Clouds, Journal of Atmospheric Sciences, 52, 2058-2072, doi:10.1175/1520-0469(1995)052<2058:MRTTCC>2.0.CO;2, 1995b.

Evans, K. F., Walter, S. J., Heymsfield, A. J., and Deeter, M. N.: Modeling of Submillimeter Passive Remote Sensing of Cirrus Clouds, Journal of Applied Meteorology, 37, 184-205, doi:10.1175/1520-0450(1998)037<0184:MOSPRS>2.0.CO;2, 1998.

Evans, K. F., Walter, S. J., Heymsfield, A. J., and McFarquhar, G. M.: Submillimeter-Wave Cloud Ice Radiometer: Simulations of retrieval algorithm performance, Journal of Geophysical Research: Atmospheres, 107, AAC 2-1-AAC 2-21, doi:10.1029/2001JD000709, 2002.

Forster, P., Storelvmo, T., Armour, K., Collins, W., Dufresne, J. L., Frame, D., Lunt, D. J., Mauritsen, T., Palmer, M. D., Watanabe, M., Wild, M., and Zhang, H.: The Earth's Energy Budget, Climate Feedbacks, and Climate Sensitivity, in: Climate Change 2021: The Physical Science Basis. Contribution of Working Group I to the Sixth Assessment Report of the Intergovernmental Panel on Climate Change, edited by: Masson-Delmotte, V., Zhai, P., Pirani, A., Connors, S. L., Péan, C., Berger, S., Caud, N., Chen, Y., Goldfarb, L., Gomis, M. I., Huang, M., Leitzell, K., Lonnoy, E., Matthews, J. B. R., Maycock, T. K., Waterfield, T., Yelekçi, O., Yu, R., and Zhou, B., Cambridge University Press, Cambridge, United Kingdom and New York, NY, USA, 923–1054, doi:10.1017/9781009157896.009, 2021.

https://doi.org/10.5194/amt-2022-247
Preprint. Discussion started: 8 September 2022
© Author(s) 2022. CC BY 4.0 License.

Atmospheric Measurement Techniques Discussions

Fox, S., Mendrok, J., Eriksson, P., Ekelund, R., amp, apos, Shea, S., Bower, K., Baran, A., Harlow, C., and Pickering, J.: Airborne validation of radiative transfer modelling of ice clouds at millimetre and sub-millimetre wavelengths, Atmospheric Measurement Techniques, 12, 1599-1617, doi:10.5194/amt-12-1599-2019, 2019.

Fox, S., Lee, C., Moyna, B., Philipp, M., Rule, I., Rogers, S., King, R., Oldfield, M., Rea, S., Henry, M., Wang, H., and Harlow, C.: ISMAR: An airborne submillimetre radiometer, Atmospheric Measurement Techniques, 10, 477-490, doi:10.5194/amt-10-477-2017, 2017.

Fu, Q., Sun, W. B., and Yang, P.: Modeling of scattering and absorption by nonspherical cirrus ice particles at thermal infrared wavelengths, J Atmos Sci, 56, 2937-2947, doi:10.1175/1520-0469(1999)056<2937:MOSAAB>2.0.CO;2, 1999.

Gao, T., Li, S., Liu, L., and Huang, W.: Development study of THz instruments for atmospheric sounding, Infrared and Laser Engineering, 45, 56-67, doi:10.3788/IRLA201645.0425002, 2016.

Gasiewski, A. J.: Numerical sensitivity analysis of passive EHF and SMMW channels to tropospheric water vapor, clouds, and precipitation, IEEE Transactions on Geoscience and Remote Sensing, 30, 859-870, doi:10.1109/36.175320, 1992.

Hans, H., Bell, W., Berrisford, P., Andras, H., Muñoz-Sabater, J., Nicolas, J., Raluca, R., Dinand, S., Adrian, S., Cornel, S., and Dick, D.: Global reanalysis: goodbye ERA-Interim, hello ERA5, doi:10.1002/qj.3803, 2019.

Heymsfield, A. J., Schmitt, C., and Bansemer, A.: Ice Cloud Particle Size Distributions and Pressure-Dependent Terminal Velocities from In Situ Observations at Temperatures from 0° to −86°C, J Atmos Sci, 70, 4123-4154, doi:10.1175/JAS-D-12-0124.1, 2013.

Heymsfield, A. J., Krämer, M., Luebke, A., Brown, P., Cziczo, D. J., Franklin, C., Lawson, P., Lohmann, U., McFarquhar, G., Ulanowski, Z., and Van Tricht, K.: Cirrus Clouds, Meteorological Monographs, 58, 2.1-2.26, doi:10.1175/AMSMONOGRAPHS-D-16-0010.1, 2017.

Hong, Y., Liu, G., and Li, J. L. F.: Assessing the Radiative Effects of Global Ice Clouds Based on CloudSat and CALIPSO Measurements, Journal of Climate, 29, 7651-7674, doi:10.1175/JCLI-D-15-0799.1, 2016.

Illingworth, A. J., Barker, H. W., Beljaars, A., Ceccaldi, M., Chepfer, H., Clerbaux, N., Cole, J., Delanoe, J., Domenech, C., Donovan, D. P., Fukuda, S., Hirakata, M., Hogan, R. J., Huenerbein, A., Kollias, P., Kubota, T., Nakajima, T., Nakajima, T. Y., Nishizawa, T., Ohno, Y., Okamoto, H., Oki, R., Sato, K., Satoh, M., Shephard, M. W., Velazquez-Blazquez, A., Wandinger, U., Wehr, T., and van Zadelhoff, G.-J.: THE EARTHCARE SATELLITE The Next Step Forward in Global Measurements of Clouds, Aerosols, Precipitation, and Radiation, B Am Meteorol Soc, 96, 1311-1332, doi:10.1175/BAMS-D-12-00227.1, 2015.

Inatani, J., Ozeki, H., Satoh, R., Nishibori, T., Ikeda, N., Fujii, Y., Nakajima, T., Iida, Y., Iida, T., Kikuchi, K., Miura, T., and Masuko, H.: Submillimeter limb-emission sounder JEM/SMILES aboard the Space Station, Proc SPIE, doi:10.1117/12.410604, 2000.

Ishimoto, H., Masuda, K., Mano, Y., Orikasa, N., and Uchiyama, A.: Irregularly shaped ice aggregates in optical modeling of convectively generated ice clouds, J Quant Spectrosc Ra, 113, 632-643, doi:10.1016/j.jqsrt.2012.01.017, 2012.

© Author(s) 2022. CC BY 4.0 License.


Ishimoto, H., Masuda, K., Mano, Y., Orikasa, N., and Uchiyama, A.: Optical Modeling of Irregularly Shaped Ice Particles in Convective Cirrus, 184-187 pp., doi:10.1063/1.4804737, 2013.

Jimenez, C., Eriksson, P., and Murtagh, D.: First inversions of observed submillimeter limb sounding radiances by neural networks, Journal of Geophysical Research, 108, doi:10.1029/2003JD003826, 2003.

Kangas, V., D'Addio, S., Klein, U., Loiselet, M., Mason, G., Orlhac, J.-C., Gonzalez, R., Bergada, M., Brandt, M., and Thomas, B.: Ice cloud imager instrument for MetOp Second Generation, 2014 13th Specialist Meeting on Microwave Radiometry and Remote Sensing of the Environment(MicroRad), 228-231, doi:10.1109/MicroRad.2014.6878946, 2014.

Lawson, R. P., Baker, B., Pilson, B., and Mo, Q. X.: In situ observations of the microphysical properties of wave, cirrus, and anvil clouds. Part II: Cirrus clouds, J Atmos Sci, 63, 3186-3203, doi:10.1175/JAS3803.1, 2006.

Lawson, R. P., Woods, S., Jensen, E., Erfani, E., Gurganus, C., Gallagher, M., Connolly, P., Whiteway, J., Baran, A. J., May, P., Heymsfield, A., Schmitt, C. G., McFarquhar, G., Um, J., Protat, A., Bailey, M., Lance, S., Muehlbauer, A., Stith, J., Korolev, A., Toon, O. B., and Kramer, M.: A Review of Ice Particle Shapes in Cirrus formed In Situ and in Anvils, J Geophys Res-Atmos, 124, 10049-10090, doi:10.1029/2018JD030122, 2019.

Letu, H., Nakajima, T. Y., and Matsui, T. N.: Development of an ice crystal scattering database for the global change observation mission/second generation global imager satellite mission: investigating the refractive index grid system and potential retrieval error, Appl Optics, 51, 6172-6178, doi:10.1364/AO.51.006172, 2012.

Letu, H., Ishimoto, H., Riedi, J., Nakajima, T. Y., Labonnote, L. C., Baran, A. J., Nagao, T. M., and Sekiguchi, M.: Investigation of ice particle habits to be used for ice cloud remote sensing for the GCOM-C satellite mission, Atmos Chem Phys, 16, 12287-12303, doi:10.5194/acpd-15-31665-2015, 2016.

Letu, H. S., Nagao, T. M., Nakajima, T. Y., Riedi, J., Ishimoto, H., Baran, A. J., Shang, H. Z., Sekiguchi, M., and Kikuchi, M.: Ice Cloud Properties From Himawari-8/AHI Next-Generation Geostationary Satellite: Capability of the AHI to Monitor the DC Cloud Generation Process, Ieee T Geosci Remote, 57, 3229-3239, doi:10.1109/TGRS.2018.2882803, 2018.

Li, M., Letu, H., Peng, Y., Ishimoto, H., Lin, Y., Nakajima, T. Y., Baran, A. J., Guo, Z., Lei, Y., and Shi, J.: Investigation of ice cloud modeling capabilities for the irregularly shaped Voronoi ice scattering models in climate simulations, Atmos. Chem. Phys., 22, 4809-4825, doi:10.5194/acp-22-4809-2022, 2022.

Li, S., Liu, L., Gao, T., Hu, S., and Huang, W.: Retrieval method of cirrus microphysical parameters at terahertz wave based on multiple lookup tables, Acta Physica Sinica, 66, 78-87, doi:10.7498/aps.66.054102, 2017.

Li, S., Liu, L., Gao, T., Huang, W., and Hu, S.: Sensitivity analysis of terahertz wave passive remote sensing of cirrus microphysical parameters, Acta Physica Sinica, 65, 100-110, doi:10.7498/aps.65.134102, 2016.

Li, S., Liu, L., Gao, T., Shi, L., Qiu, S., and Hu, S.: Radiation characteristics of the selected channels for cirrus remote sensing in terahertz waveband and the influence factors for the retrieval method, Journal of Infrared and Millimeter Waves, 37, 60-65+71, doi:10.11972/j.issn.1001-9014.2018.01.012, 2018.

Liou, K.-N.: Radiation and cloud processes in the atmosphere: theory, observation and modeling, Oxford monographs on geology and geophysics, 20, Oxford University Press, New York, ix, 487 p. pp., doi:10.1063/1.2809044, 1992.

© Author(s) 2022. CC BY 4.0 License.


Liu, L., Weng, C., Li, S., Letu, H., Hu, S., and Dong, P.: Passive Remote Sensing of Ice Cloud Properties at Terahertz Wavelengths Based on Genetic Algorithm, Remote Sensing, 13, 735, doi:10.3390/rs13040735, 2021.

Liu, L., Weng, C., Li, S., Hu, S., Ye, J., Dou, F., and Shang, J.: Review of terahertz passive remote sensing of ice clouds, Advances in Earth Science, 35, 1211-1221, doi:10.11867/j.issn.1001-8166.2020.103, 2020.

Macke, A., Mishchenko, M. I., and Cairns, B.: The influence of inclusions on light scattering by large ice particles, J Geophys Res-Atmos, 101, 23311-23316, doi:10.1029/96jd02364, 1996a.

Nakajima, T. and King, M. D.: Determination of the Optical-Thickness and Effective Particle Radius of Clouds from Reflected Solar-Radiation Measurements .1. Theory, J Atmos Sci, 47, 1878-1893, doi:10.1175/1520-0469(1990)047<1878:Dotota>2.0.Co;2, 1990.

Nakajima, T. and Tanaka, M.: Matrix formulation for the transfer of solar radiation in a plane-parallel scattering atmosphere, Journal of Quantitative Spectroscopy & Radiative Transfer - J QUANT SPECTROSC RADIAT, 35, 13-21, doi:10.1016/0022-4073(86)90088-9, 1986.

Nakajima, T. and Tanaka, M.: Algorithms for radiative intensity calculations in moderately thick atmospheres using truncation approximation, Journal of Quantitative Spectroscopy and Radiative Transfer, 40, 51-69, doi:10.1016/0022-4073(88)90031-3, 1988.

Nakajima, T., King, M. D., Spinhirne, J. D., and Radke, L. F.: Determination of the Optical-Thickness and Effective Particle Radius of Clouds from Reflected Solar-Radiation Measurements .2. Marine Stratocumulus Observations, J Atmos Sci, 48, 728-750, doi:10.1175/1520-0469(1991)048<0728:Dotota>2.0.Co;2, 1991.

Nakajima, T., Nakajima, T., Yoshimori, K., Mishra, S., and Tripathi, S.: Development of a light scattering solver applicable to particles of arbitrary shape on the basis of the surface-integral equations method of Müller type. I. Methodology, accuracy of calculation, and electromagnetic current on the particle surface, Applied optics, 48, 3526-3536, doi:10.1364/AO.48.003526, 2009.

Nakajima, T. Y. and Nakajima, T.: Wide-area determination of cloud microphysical properties from NOAA AVHRR measurements for FIRE and ASTEX regions, J Atmos Sci, 52, 4043-4059, doi:10.1175/1520-0469(1995)052<4043:Wadocm>2.0.Co;2, 1995.

Nakajima, T. Y., Ishida, H., Nagao, T. M., Hori, M., Letu, H., Higuchi, R., Tamaru, N., Imoto, N., and Yamazaki, A.: Theoretical basis of the algorithms and early phase results of the GCOM-C (Shikisai) SGLI cloud products, Prog Earth Planet Sc, 6, doi:10.1186/s40645-019-0295-9, 2019.

Platnick, S., King, M. D., Ackerman, S. A., Menzel, W. P., Baum, B. A., Riedi, J. C., and Frey, R. A.: The MODIS cloud products: algorithms and examples from Terra, IEEE Transactions on Geoscience & Remote Sensing, 41, 459-473, doi:10.1109/TGRS.2002.808301, 2003.

Platnick, S., Meyer, K. G., King, M. D., Wind, G., Amarasinghe, N., Marchant, B., Arnold, G. T., Zhang, Z. B., Hubanks, P. A., Holz, R. E., Yang, P., Ridgway, W. L., and Riedi, J.: The MODIS Cloud Optical and Microphysical Products: Collection 6 Updates and Examples From Terra and Aqua, Ieee T Geosci Remote, 55, 502-525, doi:10.1109/Tgrs.2016.2610522, 2017.

© Author(s) 2022. CC BY 4.0 License.


555 Rossow, W.: Clouds in Weather and Climate: The International Satellite Cloud Climatology Project at 30: What Do We Know and What Do We Still Need to Know?, Bulletin of the American Meteorological Society, 95, 441-443, doi:10.1175/BAMS-D-13-00138.1, 2014.

Rossow, W. B. and Schiffer, R. A.: Isccp Cloud Data Products, Bulletin of the American Meteorological Society, 72, 2-20, doi:10.1175/1520-0477(1991)072<0002:ICDP>2.0.CO;2, 1991.

560 Stephens, G. L., Li, J., Wild, M., Clayson, C. A., Loeb, N., Kato, S., L'Ecuyer, T., Stackhouse, P. W., Lebsock, M., and Andrews, T.: An update on Earth's energy balance in light of the latest global observations, Nature Geoscience, 5, 691-696, doi:10.1038/ngeo1580, 2012.

Takano, Y. and Liou, K. N.: Solar Radiative-Transfer in Cirrus Clouds .1. Single-Scattering and Optical-Properties of Hexagonal Ice Crystals, J Atmos Sci, 46, 3-19, doi:0.1175/1520-0469(1989)046<0003:SRTICC>2.0.CO;2, 1989.

565 van de Hulst, H. C.: Light scattering by small particles, Wiley, New York,, xiii, 470 p. pp., doi:10.1063/1.3060205, 1957.

Weng, C., Liu, L., Gao, T., Hu, S., Li, S., Dou, F., and Shang, J.: Multi-Channel Regression Inversion Method for Passive Remote Sensing of Ice Water Path in the Terahertz Band, Atmosphere-Basel, 10, 437, doi:10.3390/atmos10080437, 2019.

Wu, D. L., Esper, J., Ehsan, N., Piepmeier, J. R., and Racette, P.: Icecube: Spaceflight Validation of an 874-GHz Submillimeter Wave Radiometer for Ice Cloud Remote Sensing, 2014/12/1, A22F-02, doi:10.1117/12.2530589,

570 Yang, P. and Liou, K. N.: Geometric-optics-integral-equation method for light scattering by nonspherical ice crystals, Appl Optics, 35, 6568-6584, doi:10.1364/AO.35.006568, 1996a.

Yang, P. and Liou, K. N.: Finite-difference time domain method for light scattering by small ice crystals in three-dimensional space, J Opt Soc Am A, 13, 2072-2085, doi:10.1364/JOSAA.13.002072, 1996b.

Yang, P., Liou, K. N., Mishchenko, M. I., and Gao, B. C.: Efficient finite-difference time-domain scheme for light scattering

575 by dielectric particles: application to aerosols, Appl Optics, 39, 3727-3737, doi:10.1364/Ao.39.003727, 2000b.

Yang, P., Hioki, S., Saito, M., Kuo, C. P., Baum, B. A., and Liou, K. N.: A Review of Ice Cloud Optical Property Models for Passive Satellite Remote Sensing, Atmosphere-Basel, 9, doi:10.3390/atmos9120499, 2018.

Yang, P., Liou, K. N., Bi, L., Liu, C., Yi, B. Q., and Baum, B. A.: On the Radiative Properties of Ice Clouds: Light Scattering, Remote Sensing, and Radiation Parameterization, Adv Atmos Sci, 32, 32-63, doi:10.1007/s00376-014-0011-z,

580 2015.

Yang, P., Bi, L., Baum, B. A., Liou, K. N., Kattawar, G. W., Mishchenko, M. I., and Cole, B.: Spectrally Consistent Scattering, Absorption, and Polarization Properties of Atmospheric Ice Crystals at Wavelengths from 0.2 to 100 μm, J Atmos Sci, 70, 330-347, doi:10.1175/JAS-D-12-039.1, 2013.

Yee, K. S.: Numerical solution of initial boundary value problems involving maxwell's equations in isotropic media, IEEE

585 Transactions on Antennas & Propagation, 14, 302-307, doi:10.1109/TAP.1966.1138693, 1966.

Yi, B. Q., Rapp, A. D., Yang, P., Baum, B. A., and King, M. D.: A comparison of Aqua MODIS ice and liquid water cloud physical and optical properties between collection 6 and collection 5.1: Cloud radiative effects, J Geophys Res-Atmos, 122, 4550-4564, doi:10.1002/2016JD025654, 2017.

https://doi.org/10.5194/amt-2022-247
Preprint. Discussion started: 8 September 2022
© Author(s) 2022. CC BY 4.0 License.

Atmospheric Measurement Techniques Discussions

Yurkin, M. A. and Hoekstra, A. G.: The discrete dipole approximation: An overview and recent developments, J Quant Spectrosc Ra, 106, 558-589, doi:10.1016/j.jqsrt.2007.01.034, 2007.

Zhang, H., Wang, F., Zhao, S., and Xie, B.: Earth's energy budget, climate feedbacks, and climate sensitivity, Adv Clim Chang Res, 17, 691-698, doi:10.12006/j.issn.1673-1719.2021.191, 2021.

Zhao, W. J., Peng, Y. R., Wang, B., Yi, B. Q., Lin, Y. L., and Li, J. N.: Comparison of three ice cloud optical schemes in climate simulations with community atmospheric model version 5, Atmos Res, 204, 37-53, doi:10.1016/j.atmosres.2018.01.004, 2018.

https://doi.org/10.5194/amt-2022-247
Preprint. Discussion started: 8 September 2022
© Author(s) 2022. CC BY 4.0 License.

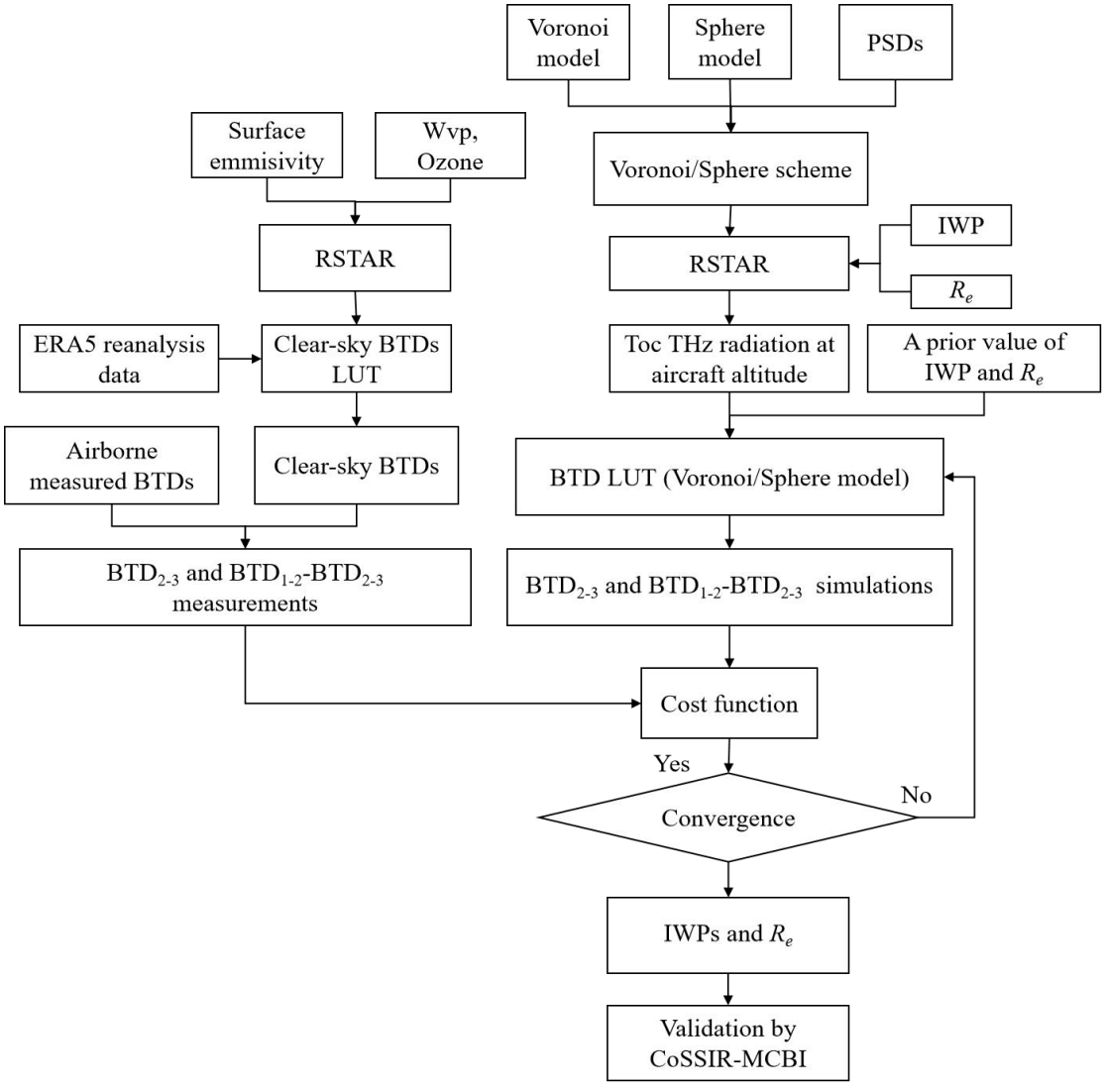

Figure 1: The overall flowchart of the retrieval of the IWP and R_e of ice clouds based on the Voronoi and Sphere ICS models.

600

https://doi.org/10.5194/amt-2022-247
Preprint. Discussion started: 8 September 2022
© Author(s) 2022. CC BY 4.0 License.

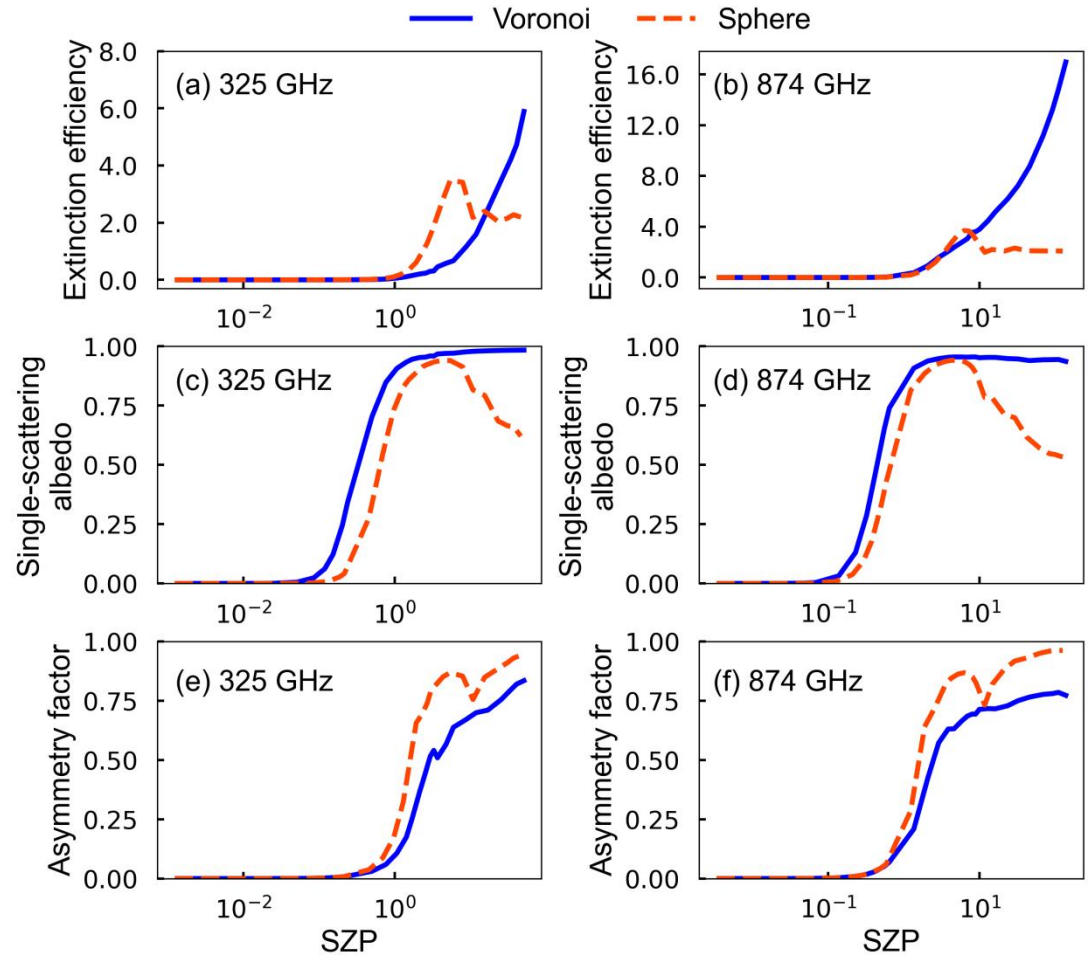

Figure 2: The extinction efficiency, single-scattering albedo and asymmetry factor as functions of the SZP for the Voronoi and Sphere ICS models in the (a, c, e) 325 and (b, d, f) 874 GHz frequencies.

https://doi.org/10.5194/amt-2022-247
Preprint. Discussion started: 8 September 2022
© Author(s) 2022. CC BY 4.0 License.

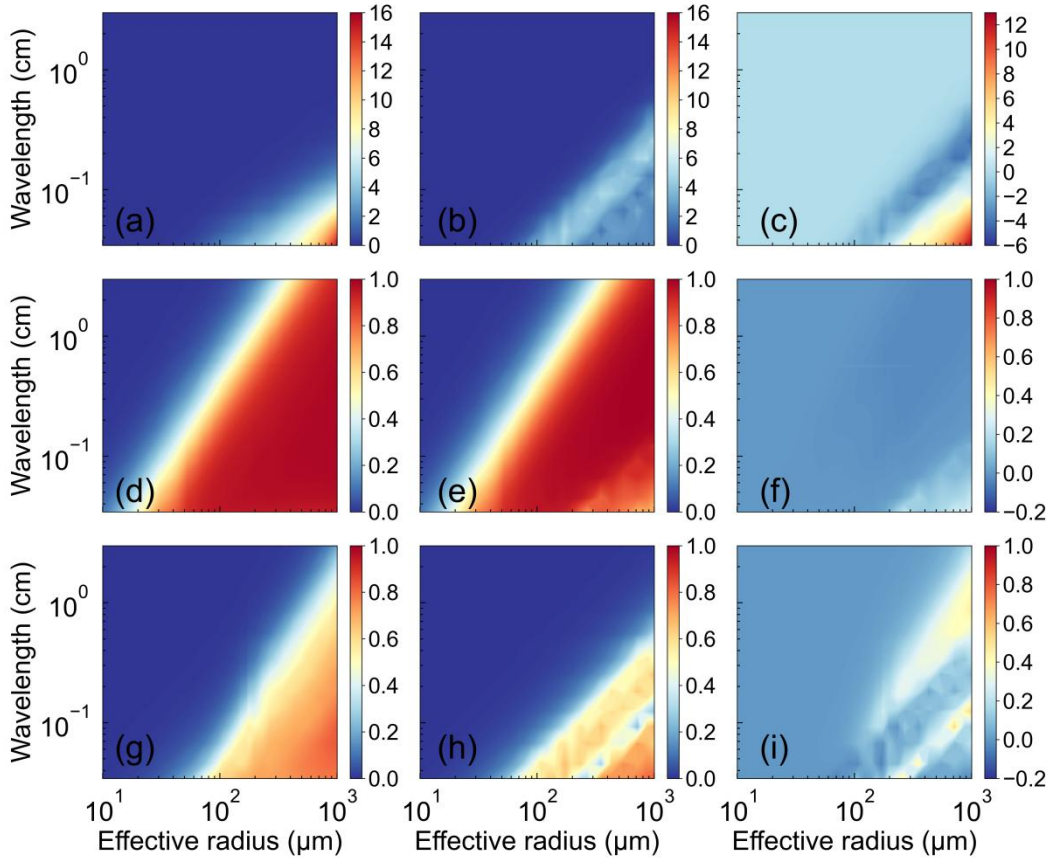

Figure 3: The comparison of the extinction efficiency, single-scattering albedo and asymmetry factor as functions of the effective radius and terahertz wavelength (0.03-3cm) for the (a, d, g) Voronoi and (b, e, h) Sphere ICS models, as well as the (c, f, i) Voronoi minus Sphere differences.

https://doi.org/10.5194/amt-2022-247
Preprint. Discussion started: 8 September 2022
© Author(s) 2022. CC BY 4.0 License.

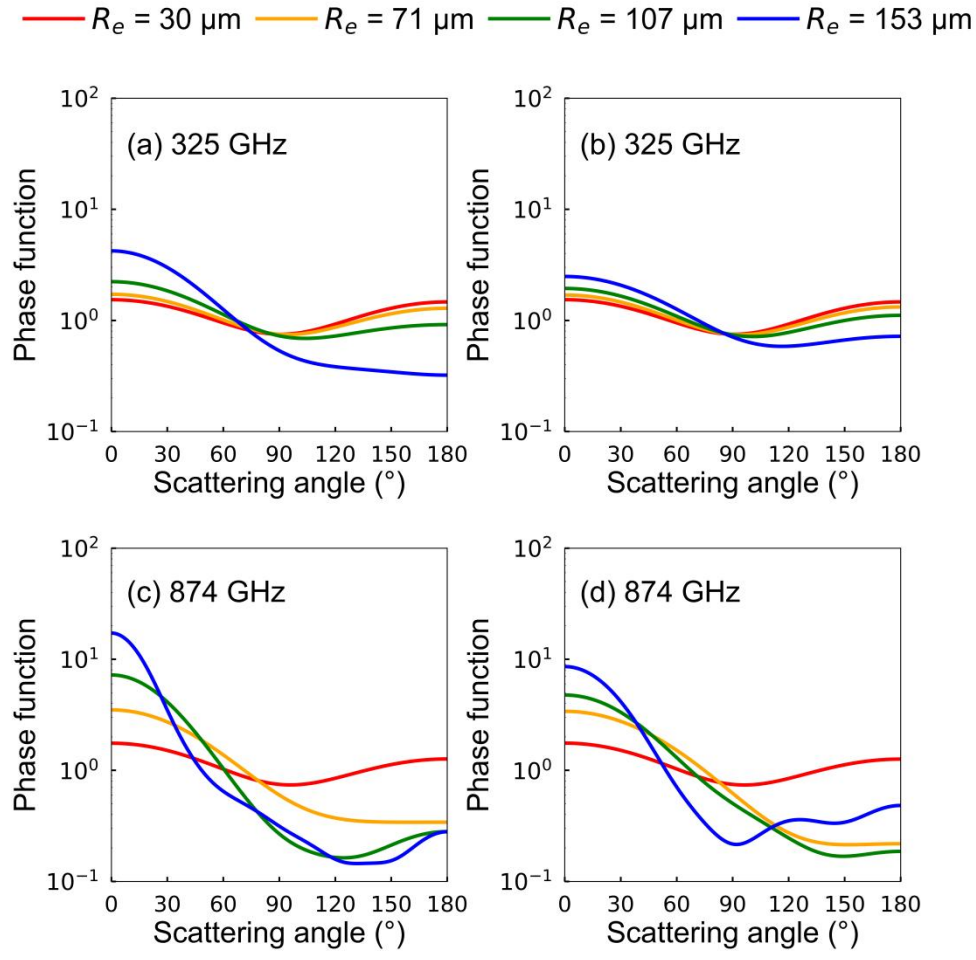

615 **Figure 4: The scattering phase functions for ice particles with four sizes (R_e = 30, 71, 107 and 153 μm) for the (a, c) Voronoi and (b, d) Sphere ICS models at 325 and 874 GHz, respectively.**

https://doi.org/10.5194/amt-2022-247
Preprint. Discussion started: 8 September 2022
© Author(s) 2022. CC BY 4.0 License.

Atmospheric Measurement Techniques Discussions

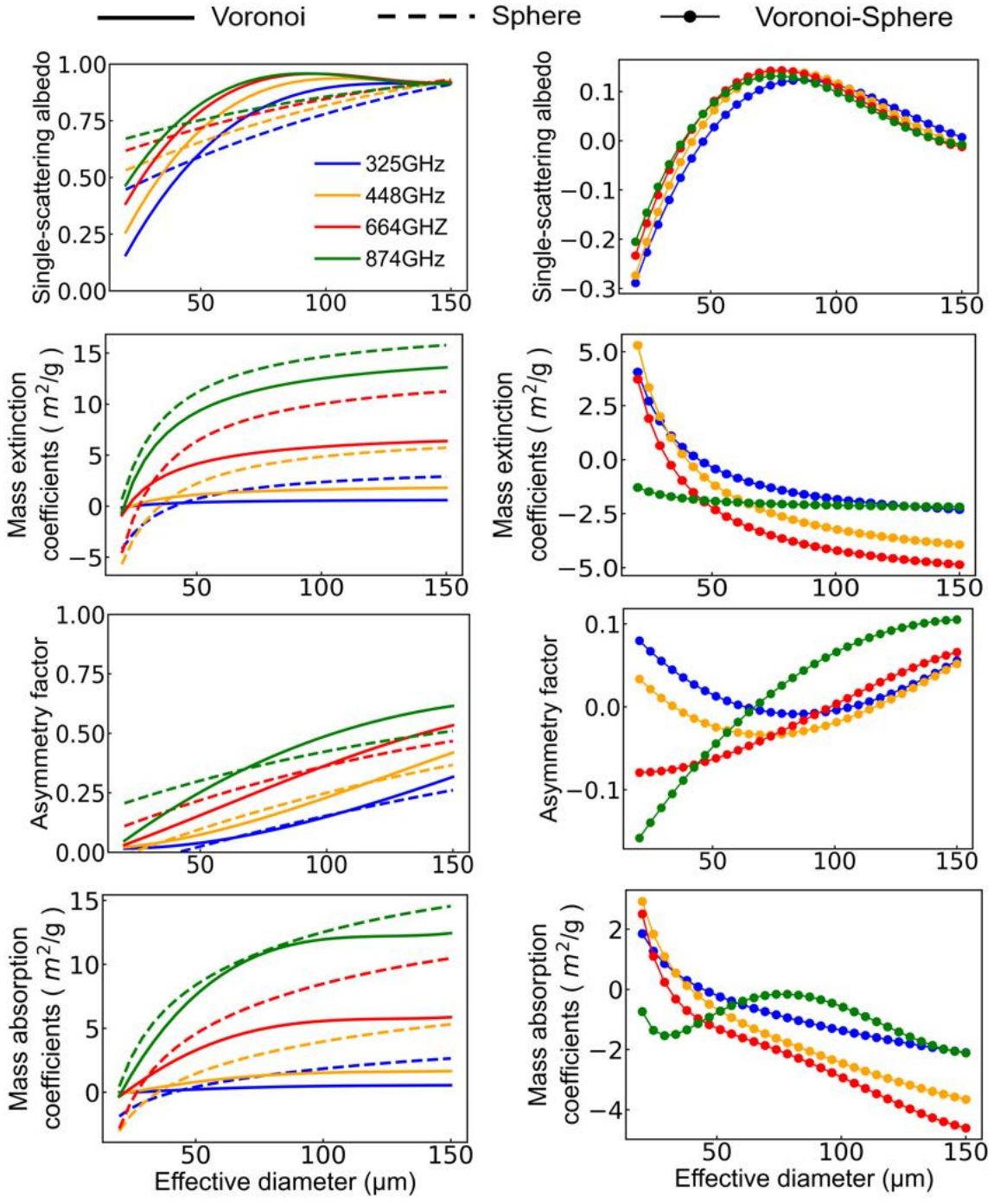

620 **Figure 5: The comparison of the single-scattering albedo, mass extinction coefficients, asymmetry factor and mass absorption coefficients as functions of effective diameters for 325, 448, 664 and 874 GHz for the Voronoi (solid line) and the Voronoi minus Sphere differences (dashed line).**

https://doi.org/10.5194/amt-2022-247
Preprint. Discussion started: 8 September 2022
© Author(s) 2022. CC BY 4.0 License.

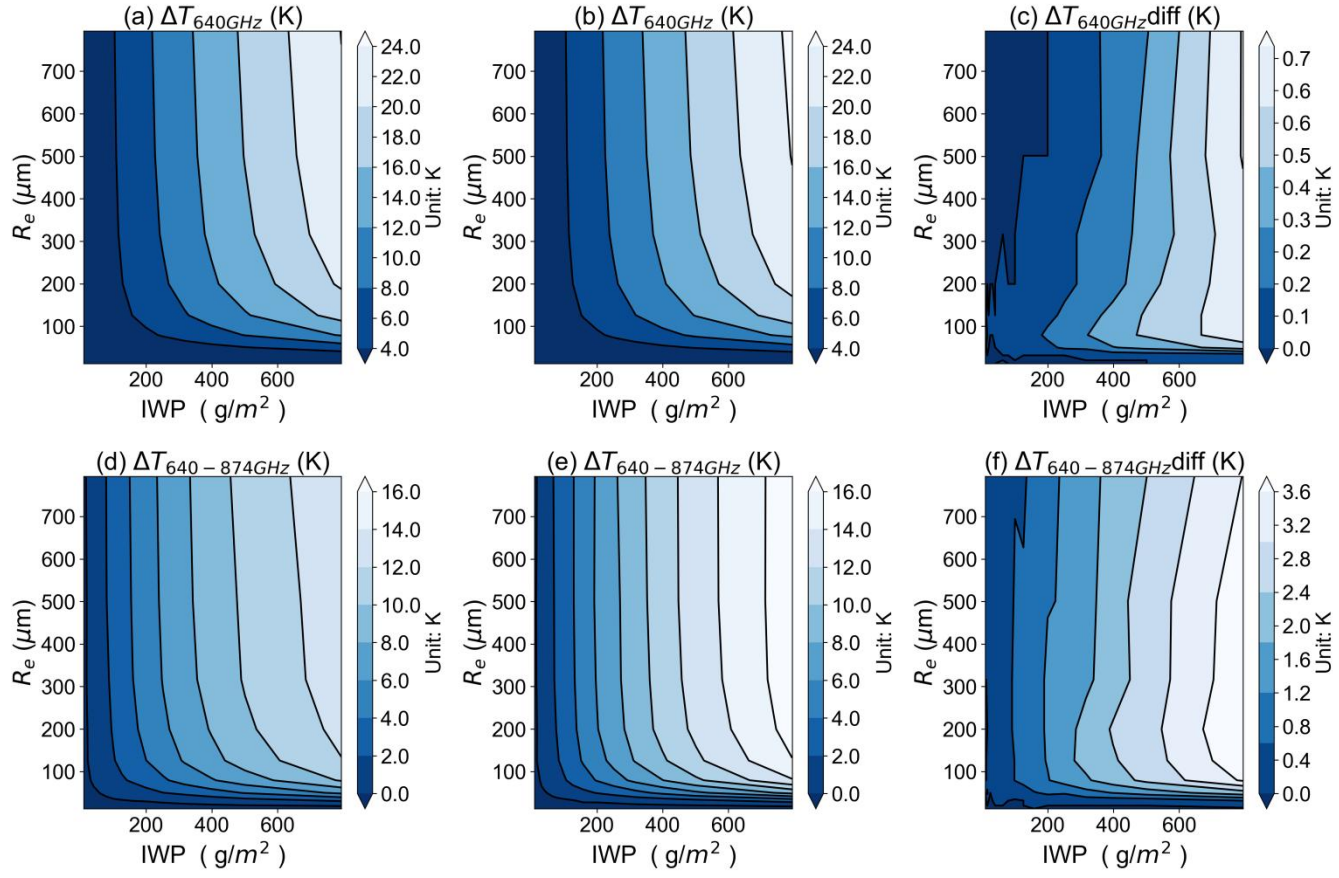

625

Figure 6: BTD_2 and $BTD_{2\text{-}3}$ for the (a, d)Voronoi, (b, e) Sphere ICS models and (c, f) Voronoi minus Sphere differences as functions of the IWP and R_e, respectively.

https://doi.org/10.5194/amt-2022-247
Preprint. Discussion started: 8 September 2022
© Author(s) 2022. CC BY 4.0 License.

Atmospheric Measurement Techniques Discussions

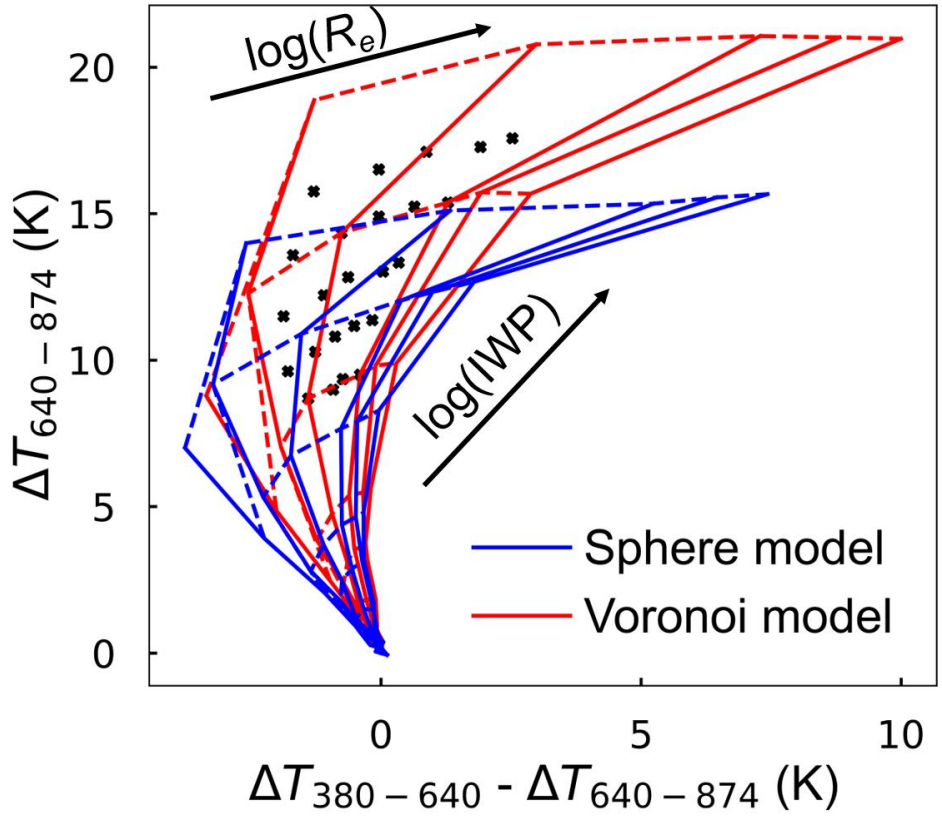

630 **Figure 7: The LUT of $BTD_{2\text{-}3}$ and $BTD_{1\text{-}2}$ - $BTD_{2\text{-}3}$ for the Voronoi and Sphere ICS models varying with the IWP and R_e. The black dots represent the randomly generated 2000 test data from RSTAR model.**

https://doi.org/10.5194/amt-2022-247
Preprint. Discussion started: 8 September 2022
© Author(s) 2022. CC BY 4.0 License.

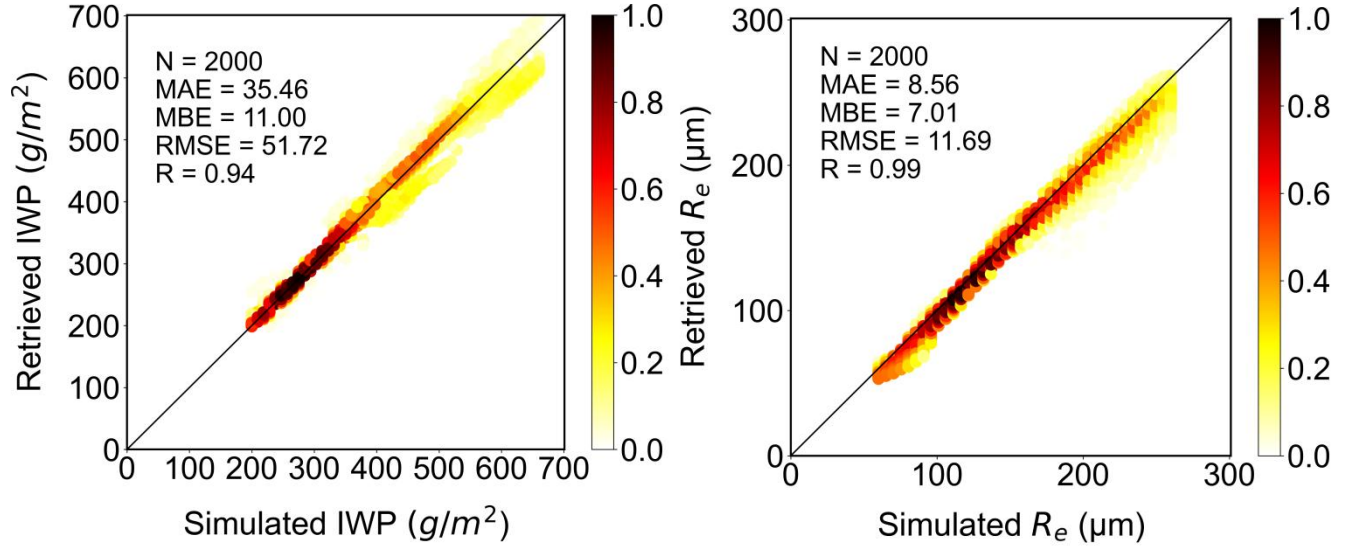

635

Figure 8: The scatterplots of the randomly generated 2000 test data and the retrieved results. The left panel and the right panel are for the IWP and R_e, respectively.

https://doi.org/10.5194/amt-2022-247
Preprint. Discussion started: 8 September 2022
© Author(s) 2022. CC BY 4.0 License.

Atmospheric Measurement Techniques Discussions

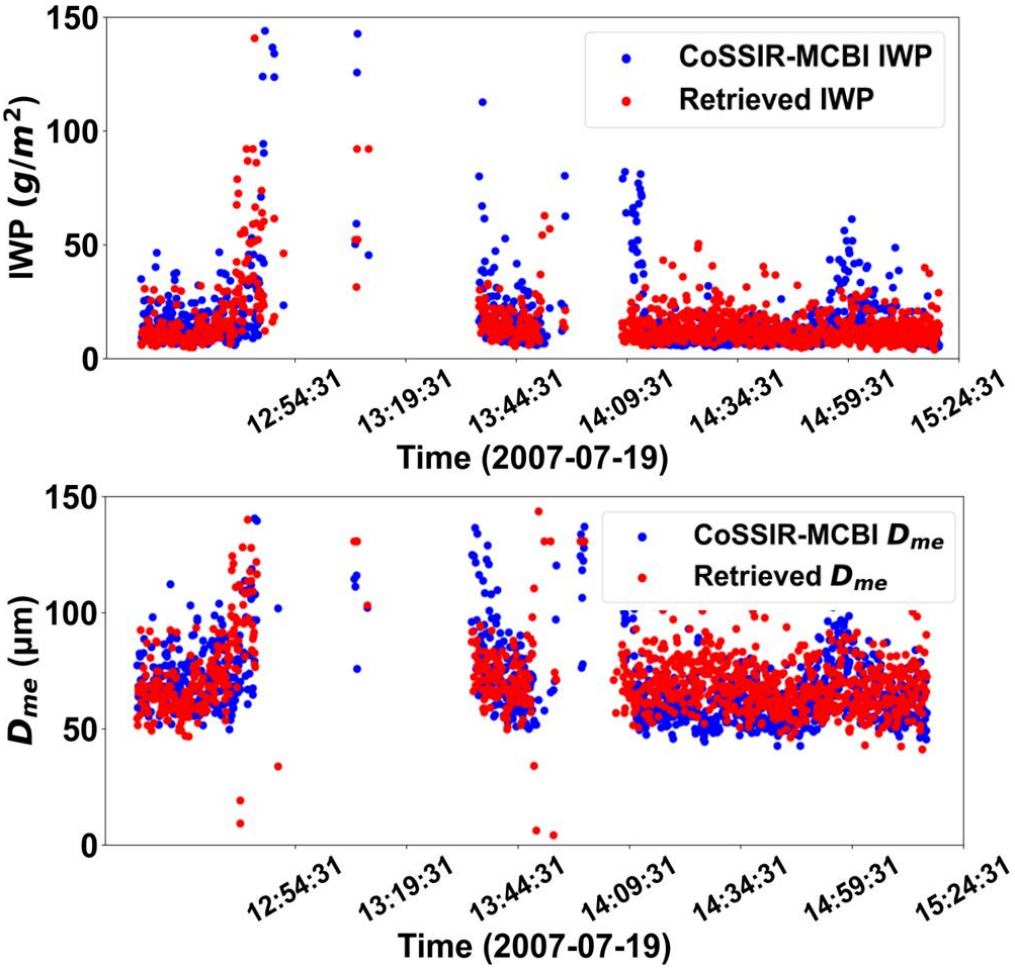

640

Figure 9: The scattered red dots are the retrieved IWP (top row) and D_{me} (bottom row) validated by the results from the CoSSIR-MCBI algorithm (blue scattered dots).

https://doi.org/10.5194/amt-2022-247
Preprint. Discussion started: 8 September 2022
© Author(s) 2022. CC BY 4.0 License.

Atmospheric Measurement Techniques Discussions

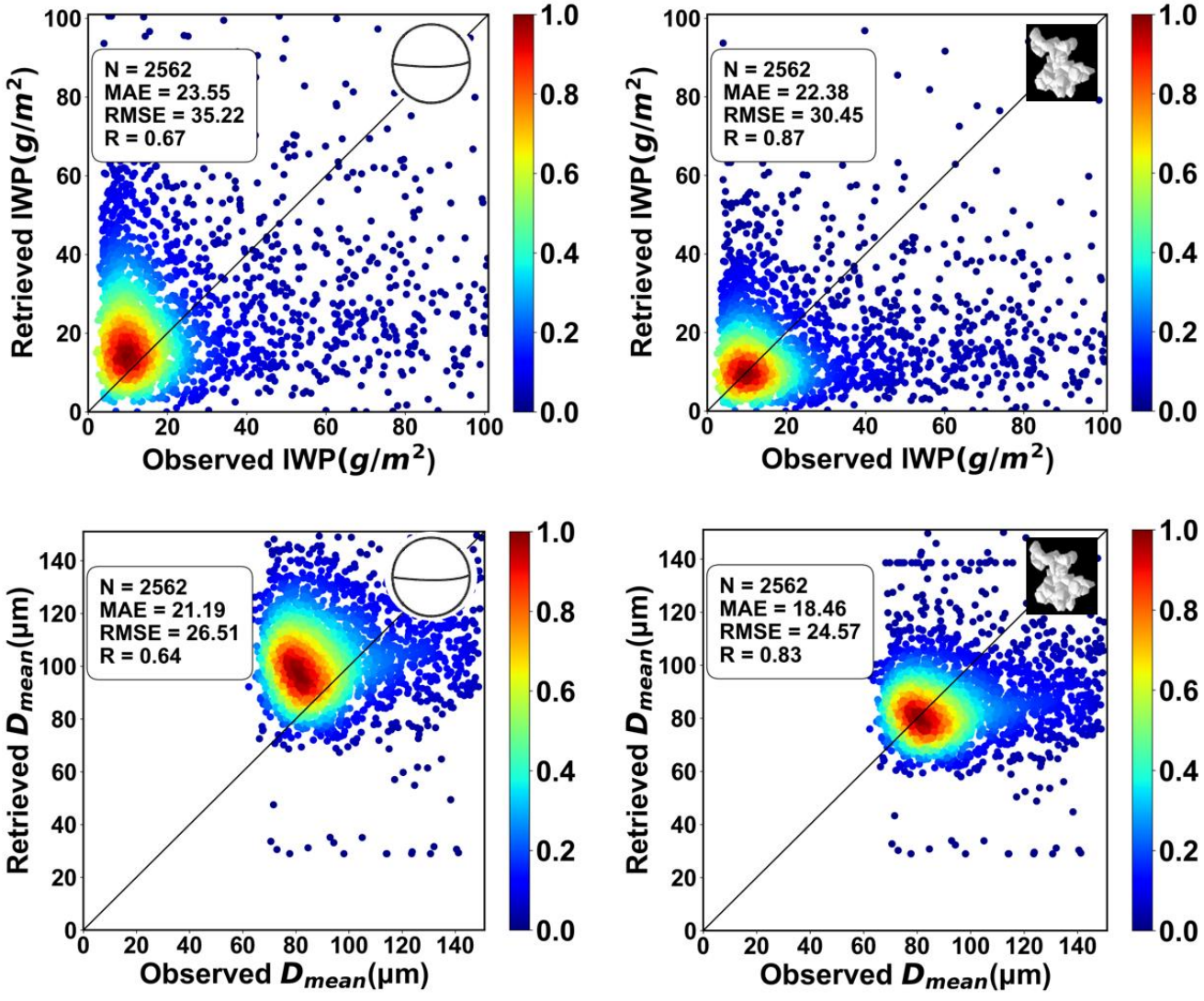

645

Figure 10: The scatterplots of the retrieved IWP (top row) and D_{me} (bottom row) against the CoSSIR-MCBI results for the Sphere (right column) and Voronoi (left column) ICS models.